Chapter 11

Thermal Radiative Wavelength Selectivity of Nanostructured Layered Media

Yi Zheng

Additional information is available at the end of the chapter

http://dx.doi.org/10.5772/67395

Abstract

Thermal radiative transport yields unique thermal characteristics of microscopic thin films—wavelength selectivity. This chapter focuses on a methodology about adjusting the wavelength selectivity of thin films embedded with nanoparticles in the far-field and near-field regimes. For nanostructured layered media doped with nanoparticles, Maxwell-Garnett-Mie theory is applied to determine the effective dielectric function for the calculation of radiative thermal transport. The thermal radiative wavelength selectivity can be affected by volume fraction and/or the size of the embedded nanoparticles in thin films. To characterize wavelength selectivity and optical property of nanostructured materials, both real and imaginary parts of effective refractive index need to be analyzed. It has been shown that the nanoparticles made of polar or metallic materials have different influence on thermal radiative wavelength selectivity of microscopic thin films.

Keywords: thermal radiation, wavelength-selective, far field, near field, nanostructured layered media

1. Introduction

Most naturally occurring materials exhibit a broad range of emission spectrum. However, thermal and optical properties of nanomaterials and nanostructures are significantly different than that of bulk materials. They are the basis of development of selective thermal emitters and absorbers that are crucial for the development of solar cells and thermophotovoltaics (TPVs) [1]. Wavelength-selective emitters also have a wide range of potential applications such as biosensors, chemical sensors [2, 3], thermal cooling, and thermal detectors [4]. It has been shown that one-dimensional (1-D) metallo-dielectric periodic structures display great selective

emission properties in the infrared and visible regions [5]. Multilayered structures of thin films (1-D photonic crystals) of polar materials can also be used to develop selective emitters [6]. The property of multilayered structures to exhibit wavelength selectivity can be explained by the presence of surface phonon polaritons (SPhPs) for polar materials and surface plasmon polaritons (SPPs) for metals [5, 7]. It has also been demonstrated that two-dimensional (2-D) or three-dimensional (3-D) photonic crystals can be used to develop selective emitters [8, 9]. However, thin-film-layered structures are easy to design and fabricate. Calculation of their emission spectra is also relatively simple.

Wavelength selectivity of 1-D photonic crystals is a far-field phenomenon. When the distance between two objects is of the order of the dominant thermal wavelength, the radiative heat transfer is enhanced to many orders of magnitude due to the coupling of surface waves and is referred to as near-field thermal radiation [10]. If the materials support SPhPs or SPPs, the near-field radiative flux can be shown to be inversely proportional to the square of the distance. The enhancement of heat transfer does not take place at all wavelengths but only at specific wavelengths [10]. This wavelength selectivity in the near field is exhibited by thin films as well as bulk materials. Wavelength selectivity in the near-field limit is due to the coupling of SPPs or SPhPs across the two surfaces [10].

While many articles dedicated to the design and fabrication of selective emitters can be found in the literature, the use of nanoparticles specifically for the application of selective emitters is relatively sparse [11]. Optical properties of materials doped with nanoparticles have been investigated before [12, 13]. Experimental and analytical study of thermal coatings doped with nanoparticles such as Gonome et al. [14, 15] can also be found in literature. However, emissive properties of nanoparticles embedded thin films have not been studied in detail to the best of our knowledge. This chapter presents the multilayered structures, which contain nanoparticles (NPs) doped into the thin films, which are suitable for any of the potential applications in both the far field and the near field. In this chapter, we investigate a methodology that can be used to develop selective thermal emitters for a desired wavelength band. Ideally, one may want to develop a selective emitter for specific wavelength band as per the requirements. As the emission spectrum displays peaks at the wavelengths, which are characteristics of the refractive index of the material, changing the thickness of the film allows control over only a narrow spectral band. We propose to dope the top layer (thin film) with nanoparticles to change the dielectric properties of the material. The usual Maxwell-Garnett equation for effective medium approximation is often employed for such an analysis disregarding the sizes of doped materials [16]. Here, we apply the Maxwell-Garnett-Mie formulation [17] for effective medium approximation to calculate the dielectric function of a composite that consists of a host material embedded with nanoparticles of various sizes and volume fractions, and extend the same approach to calculate radiative heat transfer for thin films doped with nanoparticles. Thin-film structure with nanoparticles would be easy to fabricate as submicron thin films embedded with nanoparticles have been fabricated before [18, 19]. We aim to study the effect on the wavelength selectivity of thin films due to combination of surface polaritons of the films and the nanoparticles and their effects in the near-field radiative heat transfer and spectral heat flux. We consider hypothetical cases of thin film embedded with nanoparticles although the

http://dx.doi.org/10.5772/67395

fabrication of these particular NP-embedded films discussed here is relatively unknown. We choose SiC and polystyrene (PS) as the host materials (for thin films). SiC is chosen as a host because it has high permittivity in the infrared region and supports SPhP. Polystyrene is chosen because it does not support either SPPs or SPhPs. BN, which supports SPhP, and Au, which supports SPPs, are picked for the material of inclusion (NPs).

The structure of this chapter is as follows. In Section 2, we present the theoretical background and analytical expressions used for the calculation of emissivity of thin-film structures, calculation of heat transfer between closely placed half spaces, and the application of Maxwell-Garnett-Mie theory. In Section 3, we discuss the results of our calculations obtained using the formulations outlined in Section 2. Subsequently, the ideas and conclusions of this chapter are narrated in Section 4.

2. Theoretical fundamentals

Consider a structure having N-layer media having (N - 1) interfaces. By solving the boundary conditions at the interfaces, one can obtain the expression for the generalized reflection coefficient at the interface between region i and region i + 1 and is given by [20]

$$\tilde{R}_{i,i+1}^{(\mu)} = \frac{R_{i,i+1}^{(\mu)} + \tilde{R}_{i+1,i+2}^{(\mu)} e^{2jk_{i+1,z}(d_{i+1}-d_i)}}{1 + R_{i,i+1}^{(\mu)} \tilde{R}_{i+1,i+2}^{(\mu)} e^{2jk_{i+1,z}(d_{i+1}-d_i)}} \tag{1}$$

where $j = \sqrt{-1}$, $R_{i,i+1}^{(\mu)}$ is the Fresnel reflection coefficient at the interface between the layer i and i + 1, and $\tilde{R}_{i+1,i+2}^{(\mu)}$ is the generalized reflection coefficient at the interface between the layer i + 1 and i + 2, μ = s (or p) refers to transverse electric (or magnetic) polarization, z = - d_i is the location of the ith interface. $k_{i,z} = \sqrt{\varepsilon_i(\omega)\omega^2/c^2 - k_\rho^2}$ is the normal z-component of the wave vector in medium i wherein $\varepsilon_i(\omega)$ is the relative permittivity of the medium i as a function of angular frequency ω, c is the speed of light in vacuum, and k_ρ is the magnitude of the in-plane wave vector. With $\tilde{R}_{N,N+1}^{(\mu)}$ = 0, the above equation provides a recursive relation to calculate the reflection coefficients $\tilde{R}_{i,i+1}^{(\mu)}$ in all regions. The generalized transmission coefficient for the layered slab is given by

$$\tilde{T}_{1,N}^{(\mu)} = \prod_{i=1}^{N-1} e^{2jk_{iz}(d_i - d_{i-1})} S_{i,i+1}^{(\mu)} \tag{2}$$

where $S_{i,i+1}^{(\mu)} = T_{i,i+1}^{(\mu)} / \left(1 - R_{i,i+1}^{(\mu)} \tilde{R}_{i+1,i+2}(\mu) e^{2jk_{i+1,z}(d_{i+1}-d_i)}\right)$. Alternatively, the generalized reflection and transmission coefficients can also be calculated using transfer matrix approach [21]. The hemispherical emissivity is given by the expression [6]

$$e(\omega) = \frac{c^2}{\omega^2} \int_0^{\omega/c} dk_\rho k_\rho \sum_{\mu=s,p} \left(1 - \left|\tilde{R}_{h1}^{(\mu)}\right|^2 - \left|\tilde{T}_{h1}^{(\mu)}\right|^2\right) \tag{3}$$

where $\tilde{R}_{h1}^{(\mu)}$ and $\tilde{T}_{h1}^{(\mu)}$ are the polarized effective reflection and transmission coefficients, respectively, as shown in **Figure 1(a)**.

Far-field radiative heat transfer is described by Planck's law of thermal radiation [22]. This description, however, does not account for the presence of evanescent (surface) waves that dominate only near the boundaries. The expression of radiative transfer between closely spaced objects can be derived using dyadic Green's function formalism [23], and is given by

$$q_{1\to2}(T_1, T_2, L) = \int_0^{\infty} \frac{d\omega}{2\pi} [\theta(\omega, T_1) - \theta(\omega, T_2)] T_{1\to2}(\omega, L) \tag{4}$$

where $\theta(\omega, T) = (\hbar\omega/2)coth(\hbar\omega/2k_BT)$ is the energy of harmonic oscillator at frequency ω and temperature T, h is the reduced Planck constant, and k_B is the Boltzmann constant. The function $T_{(1\to2)}$ (ω) corresponds to the spectral transmissivity in radiative transfer between media 1 and 2 separated by distance L and is expressed as [23]

$$\begin{aligned} T_{1\to2}(\omega) = & \int_0^{\omega/c} \frac{dk_\rho k_\rho}{2\pi} \sum_{\mu=s,p} \frac{\left(1 - \left|\tilde{R}_{h1}^{(\mu)}\right|\right)^2 \left(1 - \left|\tilde{R}_{h2}^{(\mu)}\right|\right)^2}{\left|1 - \tilde{R}_{h1}^{(\mu)} \tilde{R}_{h2}^{(\mu)} e^{2jk_{hz}L}\right|^2} \\ & + \int_{\omega/c}^{\infty} \frac{dk_\rho k_\rho}{2\pi} \sum_{\mu=s,p} \frac{4\mathrm{Im}\left(\tilde{R}_{h1}^{(\mu)}\right) \mathrm{Im}\left(\tilde{R}_{h2}^{(\mu)}\right) e^{-2|k_{hz}|L}}{\left|1 - \tilde{R}_{h1}^{(\mu)} \tilde{R}_{h2}^{(\mu)} e^{2jk_{hz}L}\right|^2} \end{aligned} \tag{5}$$

where $\tilde{R}_{h1}^{(\mu)}$ and $\tilde{R}_{h2}^{(\mu)}$ are polarized k_{hz} effective reflection coefficients of the two half spaces (calculated in the absence of other half space) and is the z-component of wave vector in

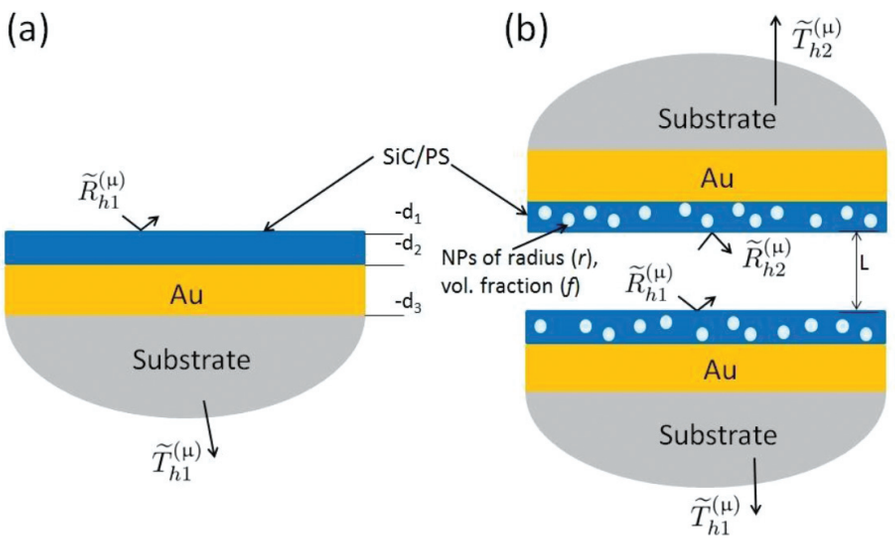

Figure 1. Configurations of nanoparticle-embedded thin films. (a) Thin film of SiC or polystyrene (PS) on Au thin film of thickness 1 μm, and (b) two half spaces with multilayers with vacuum in between. The top is SiC or PS film embedded with nanoparticles of varying radius and volume fraction on Au thin film.

vacuum. The first term in Eq. (5) corresponds to propagating waves, whereas the second term describes the thermal transport due to evanescent waves, and its contribution is significant only for small values of gap L.

Clausius-Mossotti equation for the effective dielectric function, of the composite medium containing nanoparticle inclusions in a host material, is given by [24, 25]

$$\varepsilon_{eff} = \varepsilon_m \left(\frac{r^3 + 2\alpha_r f}{r^3 - \alpha_r f} \right) \tag{6}$$

where ε_m is the dielectric function of the matrix, α_r is the electric dipole polarizability, and r and f are the radius and volume fraction of nanoparticles, respectively. The size-dependent extension of Maxwell-Garnett formula can be obtained by deriving an expression for electric dipole polarizability using Mie theory [17]

$$\alpha_r = \frac{3jc^3}{2\omega^3 \varepsilon_m^{3/2}} a_{1,r} \tag{7}$$

where $a_{1,r}$ is the first electric Mie coefficient given by

$$a_{1,r} = \frac{\sqrt{\varepsilon_{\mathrm{np}}}\psi_1(x_{\mathrm{np}})\psi_1{}'(x_m) - \sqrt{\varepsilon_m}\psi_1(x_m)\psi_1{}'(x_{\mathrm{np}})}{\sqrt{\varepsilon_{\mathrm{np}}}\psi_1(x_{\mathrm{np}})\xi_1{}'(x_m) - \sqrt{\varepsilon_m}\xi_1(x_m)\psi_1{}'(x_{\mathrm{np}})} \tag{8}$$

where ψ_1 and ξ_1 are Riccati-Bessel functions of the first order given by $\psi_1(x) = x\, j_1(x)$ and $\xi_1(x) = x h_1^{(1)}(x)$, where j_1 and $h_1^{(1)}$ are the first-order spherical Bessel functions and spherical Hankel functions of the first kind, respectively. Here, "′" indicates the first derivative. $x_m = \omega r\sqrt{\varepsilon_m}/c$ and $x_{np} = \omega r\sqrt{\varepsilon_{np}}/c$ are the size parameters of the matrix and the nanoparticles, respectively; $\varepsilon_{\mathrm{np}}$ being the dielectric function of nanoparticles.

Effective medium approximation method is applicable when average distance between inclusions is much smaller than the wavelength of interest. If the dielectric inclusions of radius r can be imagined to be arranged in simple cubic lattice of lattice constant a, the condition for validity of the effective medium approximation is $\lambda_h >> a > 2r$. Where λ_h is the wavelength in the host material [26]. We emphasize that since we use the approximation for thin films doped with nanoparticles, its use may not be correct when the particle size is comparable to the thickness of the films. Also, as discussed by Liu et al. [27], it can be argued that the use of effective medium theory (EMT) is questionable at nanoscale distances. Although such might be the case for the near-field calculations presented here, its detailed analysis is beyond the scope of this work and is left for future work. Despite the limitations of Maxwell-Garnett-Mie theory sand its application in the near-field regime, the results obtained should provide general trends and give considerable insight into optical properties of artificial materials. Further investigations by direct numerical simulation may be necessary to confirm the validity of EMT [28]. Moreover, these results will be constructive when judging the validity of the EMT in the near field by direct numerical calculations. We would like to keep these points open for speculation.

3. Results

The dielectric function is related to real (n) and imaginary (κ) parts of refractive index as $\sqrt{\varepsilon} = n + j\kappa$. For SiC and BN, the dielectric function has the form as [29, 30]

$$\varepsilon(\omega) = \varepsilon_\infty \left(\frac{\omega^2 - \omega_{LO}^2 + j\omega\gamma}{\omega^2 - \omega_{TO}^2 + j\omega\gamma} \right) \tag{9}$$

where ω_{TO} and ω_{LO} are transverse and longitudinal optical phonon frequencies, respectively, and γ is the damping constant. For SiC, the constants ε_∞, ω_{TO}, ω_{LO}, and γ are equal to 6.7, 9.83 × 10^{-2} eV, 0.12 eV, and 5.90 × 10^{-2} eV, respectively. The values of ε_∞, ω_{TO}, ω_{LO}, and γ for BN are 4.46, 0.1309 eV, 0.1616 eV, and 6.55 × 10^{-2} eV, respectively. Data for the bulk gold (Au) are taken from Johnson and Christy [31]. **Figure 2(a)** considers the case of SiC film doped with NPs of BN. SiC film of 0.4 μm is on the top of Au film of 1 μm deposited on a substrate. The effect of change in NPs volume fraction (f) is studied. The volume fraction of BN nanoparticles is changed from 0% to 30% while maintaining the radius of 25 nm. Thin film of pure SiC exhibits emission peaks at $\lambda_n^{\mathrm{SiC}} \approx 10.33$ μm and $\lambda_n^{\mathrm{SiC}} \approx 13$ μm. λ_n is the wavelength at which the real part of the refractive index becomes zero (zero-index material) [6, 32]. λ_κ is the wavelength at which the real part of refractive index (n) is large while the imaginary part of refractive index (κ) is small [6]. These peaks are attributed to the presence of SPhPs, and the characteristic wavelengths of the dielectric function of SiC. The appearance of new peaks upon 5% inclusion of BN nanoparticles has been observed at $\lambda \approx 8.5$ μm and $\lambda \approx 11.5$ μm. When the volume fraction of NPs is increased further, each of these peaks splits into two giving rise to a total of six peaks. Locations of these peaks do not correspond to the characteristic wavelengths of BN ($\lambda_n^{\mathrm{BN}} \approx 7.6$ μm and $\lambda_\kappa^{\mathrm{BN}} \approx 9.8$ μm). In addition, there exists a small shift in the emission peak at $\lambda_\kappa^{\mathrm{SiC}}$. This suggests an interaction between SiC matrix and BN NPs. Consider the case with 30% inclusion of BN. **Figure 3(a)** shows that the mixture has two additional locations where the refractive index is zero ($\lambda_{n1}^{\mathrm{mixture}} \approx 8.5$ μm and $\lambda_{n2}^{\mathrm{mixture}} \approx 11.7$ μm). Moreover, at two more points n is large while imaginary part of refractive index is small, namely $\lambda_{k1}^{\mathrm{mixture}} \approx 9$ μm and $\lambda_{k2}^{\mathrm{mixture}} \approx 11.1$ μm.

These wavelengths correspond to the additional peaks. While the additional peaks are at the location of the characteristics of the refractive index of the mixture, it is interesting to note that peaks at ≈10.33 μm and ≈12.98 μm have no or little shift even at large volume fraction of 30%, because they are characteristic wavelengths of the host. Inclusion of BN leads to new SPhP leading to new peaks. **Figure 2(b)** shows the effect of Au nanoparticles in SiC thin film. When particle size is small, especially when the size is comparable to the mean free path of the free electrons, confinement effects become significant [25, 33]. The optical properties of metallic nanoparticles have shown size dependence [34]. We utilize a size-dependent dielectric function for Au nanoparticles of radius r that takes care of electron scattering, which is given by [35]

$$\varepsilon(\omega, r) = \varepsilon_b(\omega) + \frac{\omega_p^2}{\omega^2 + j\omega\gamma_0} - \frac{\omega_p^2}{\omega^2 + j\omega(\gamma_0 + Av_f/r)} \tag{10}$$

where ε_b, ω_p, v_f, and γ_0 are the bulk dielectric function, the plasma frequency, the Fermi velocity of free electrons, and the electron damping, respectively. The values of ε_b are taken

http://dx.doi.org/10.5772/67395

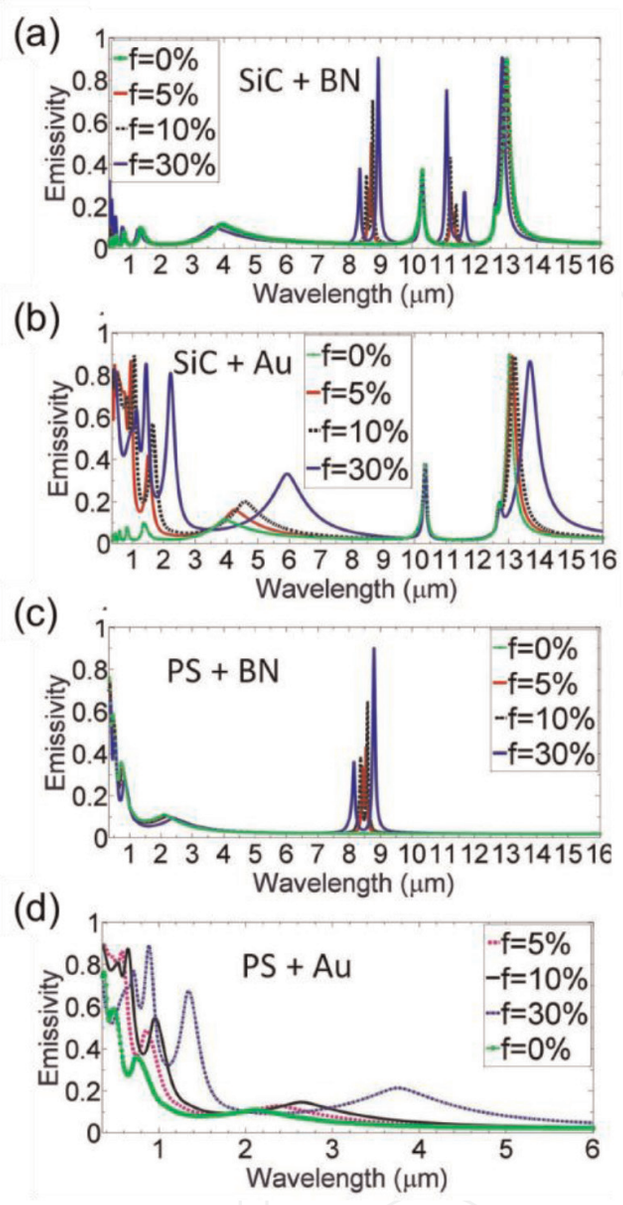

Figure 2. Emissivity spectra for SiC or PS thin film of thickness 0.4 μm embedded with BN or Au nanoparticles of radius 25 nm and various volume fractions. (a) BN nanoparticle-embedded SiC thin film, (b) Au nanoparticle-embedded SiC thin film, (c) BN nanoparticle-embedded PS thin film, and (d) Au nanoparticle-embedded PS thin film.

from Johnson and Christy [31]. The parameters ω_p, v_f, and γ_0 are taken to be 9.06 eV, 0.077 eV, and 1.4×10^6 m/s, respectively. The proportionality constant A that depends on the electron-scattering process at the surface of nanoparticles is assumed to be unity. Volume fraction is varied from 0% to 30% while NPs radius is maintained constant (25 nm). Multiple oscillatory peaks are seen in the lower wavelength region upon the addition of Au nanoparticles. A shift in the original peak of SiC at ≈13 μm is seen when volume fraction is large (30%). While the presence of a peak at ≈10.33 μm and a peak at ≈13 μm can be related to n and κ plots shown in **Figure 3(a)** and **(b)**, multiple peaks between 0.35 and 8 μm cannot be explained using the refractive index characteristics. While the change in refractive index is seen around 500 nm which corresponds to surface plasmon resonance of Au, one may expect a peak around

500 nm. Multiple peaks are observed instead. **Figure 2(c)** and **(d)** shows emission spectra of polystyrene thin film doped with BN nanoparticles and Au nanoparticles, respectively. The dielectric function of PS is in the form of [36]

$$\varepsilon(\omega) = 1 + \sum_{i=1}^{i=4} \left(\frac{f_i}{w_i^2 - \omega^2 - j g_i \omega} \right) \tag{11}$$

where the parameters f_i, w_i, and g_i are, in the units of eV, given by f_i = [14.6, 96.9, 44.4, 136.9], w_i = [6.35, 14.0, 11.0, 20.1], and g_i = [0.65, 5.0, 3.5, 11.5], respectively. In case of BN, the appearance of new peaks is quite similar to that in **Figure 2(a)** and its relation with the refractive indices shown in **Figure 4(a)** and **(b)** is obvious.

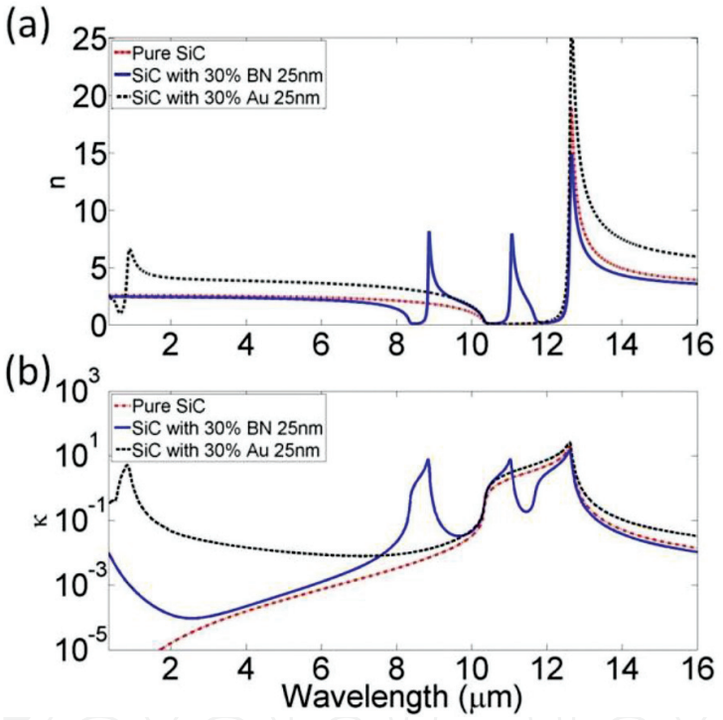

Figure 3. Refractive index of SiC and SiC film doped with 30% BN or Au nanoparticles. (a) Real part of refractive index and (b) imaginary part of refractive index.

The appearance of emission peaks at the locations of $\lambda_k^{\text{mixture}}$ and $\lambda_n^{\text{mixture}}$ is evident. However, when polystyrene film is doped with Au nanoparticles, we once again see multiple peaks produced in the region 0.35–6 μm that are not related to the refractive index characteristics. Since polystyrene does not support either of SPhPs or of SPPs, the interaction between SPPs of Au and surface polariton of the host is not responsible for the multiple peaks. We hypothesize that the origin of multiple peaks is due to the interaction of SPPs of Au and the boundaries of the thin film. In case of SiC film doped with Au nanoparticles, the shift in the peak of ≈13 μm is due to the interaction between SPPs of Au and SPhPs of SiC; in either cases (SiC and PS) the inclusion material does not produce new polaritons as seen in refractive index characteristics.

http://dx.doi.org/10.5772/67395

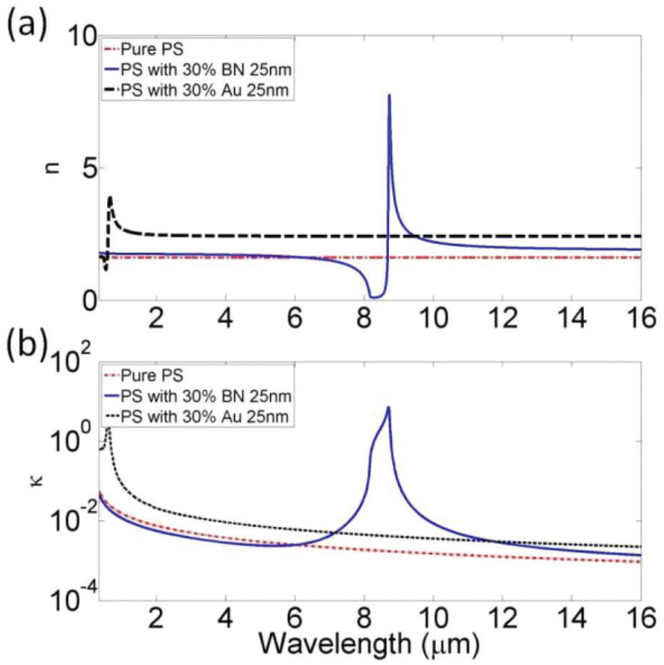

Figure 4. Refractive index of PS and PS film doped with 30% BN or Au nanoparticles. (a) Real part of refractive index and (b) imaginary part of refractive index.

Figure 5 shows the effect of NPs size on the emission spectra. In **Figure 5(a)**, SiC film of 0.4 μm is doped with BN nanoparticles and volume fraction of BN NPs is maintained constant at 10% and the radius is varied from 1 to 50 nm. The majority of emission spectrum shows no effect of BN particle size. However, the effect of size is noticeable at wavelengths less than

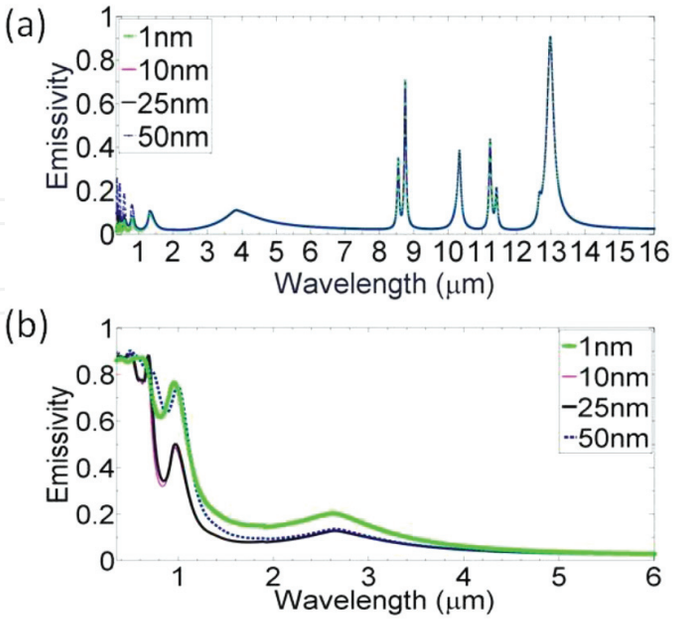

Figure 5. Emissivity spectra for SiC or PS thin film of thickness 0.4 μm embedded with BN or Au nanoparticles of volume fraction 10% and various radii. (a) BN nanoparticle-embedded SiC thin film doped and (b) Au nanoparticle-embedded PS thin film.

1 μm. This is due to the fact that Mie scattering becomes important at shorter wavelengths giving rise to higher peaks for larger particles. **Figure 5(b)** presents the calculation of emissivity for 0.4-μm thick polystyrene (PS) film doped with Au NPs. The volume fraction of NPs is fixed at 10% and the particle size is changed from 1 to 50 nm. Unlike **Figure 5(a)**, **Figure 5(b)** shows a strong influence of particle size on the emissivity. While the spectrum in the visible region shows a negligible response to particle size, gold NPs greatly influence the near-infrared region between 1 and 4 μm. As the NP size is increased from 1 nm, the emissivity peaks reduce in magnitude, showing smaller peaks for 10 and 25 nm. Emissivity for larger particles of 50 nm, however, is increased again and is comparable to that of NPs of 1 nm. This is due to the presence of two counteracting phenomena here. First is the change in dielectric function of Au NPs leading to decreased emissivity of larger particles and the second being Mie scattering of electromagnetic (EM) waves in the host causing an increased emissivity of larger particles.

Next, we present the effect of the doped nanoparticles on radiative heat transfer. We analyze radiative heat transfer between two identical multilayered structures at 300 and 301 K as shown in **Figure 1(b)**. Each structure has a top layer of 0.4 μm deposited on 1 μm of Au. The top layer is doped with nanoparticles of 25 nm and different volume fractions. **Figure 6** shows radiative heat flux versus distance between the structures and the normalized spectral density (defined as the ratio of $dq/d\omega$ to the maximum value over the range of wavelengths considered) at a distance of 100 nm is shown in the inset of figures. Consider a structure with SiC layer doped with BN nanoparticles. **Figure 6(a)** shows very little change in overall heat transfer. While thin film of pure SiC shows nearly monochromatic heat transfer, selectivity is seen at additional bands of wavelength. These locations are wavelengths where the effective refractive index of the mixture becomes zero (**Figure 3(a)** and **(b)**). While the locations of the new peaks depend on the volume fraction, the peak corresponding to the host material is relatively unchanged. In **Figure 6(b)**, SiC film is doped with Au nanoparticles of radius 25 nm with different volume fractions. The change in total heat transfer characteristics is not significant with the addition of nanoparticles. Selectivity is observed near $\lambda = \lambda_1 \approx 10.33$ μm as in Mulet et al. [10], which is one of characteristic wavelengths of SiC. Moreover, the inclusion of Au nanoparticles has only a small impact on the selectivity in the near-field limit and this can be related to the refractive indices of the mixture (**Figure 3(a)** and **(b)**). When the top layer is polystyrene doped with BN nanoparticles (**Figure 6(c)**), the near-field heat flux is clearly dependent on the volume fraction of the inclusion in both the near-field and the far-field regime. Since polystyrene does not support SPPs/SPhPs, the inclusion of BN clearly makes significant enhancement in heat transfer. The surface becomes selective at the wavelengths at which the real part of the effective refractive index becomes zero. When the PS film is doped with Au nanoparticles instead, the radiative heat transfer in **Figure 6(d)** shows an increment with an increase in NPs volume fraction, in both the near-field and the far-field limit. However, the normalized spectral density does not show any selectivity in the near field. In summary, the wavelength selectivity of thin films in the near field can be related to its effective refractive index in all four cases. This is logical as the selectivity is due to the

http://dx.doi.org/10.5772/67395

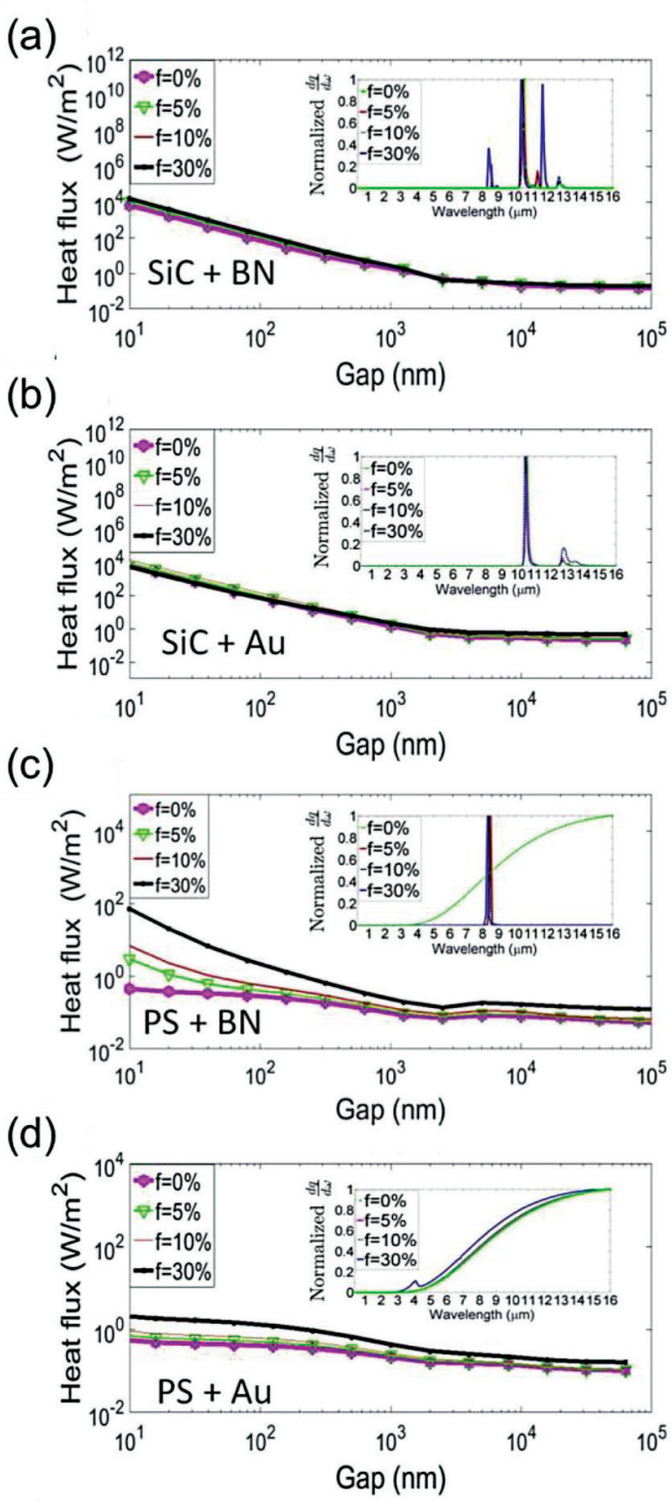

Figure 6. Heat flux of microscopic-layered media doped with BN or Au nanoparticles of radius 25 nm and various volume fractions due to near-field radiative effect. Inset: normalized spectral heat flux at a 100-nm gap between each half space with 0.4-μm thick nanoparticle-embedded layer on 1-μm Au layer. (a) BN nanoparticle-embedded SiC thin film, (b) Au nanoparticle-embedded SiC thin film, (c) BN nanoparticle-embedded PS thin film, and (d) Au nanoparticle-embedded PS thin film.

presence of SPPs/SPhPs across the interfaces. It is interesting to note that, unlike in the far-field regime, the selectivity is affected only when BN particles are used as inclusions. The addition of Au particles shows little or no impact on the selectivity in the near field. This supports the idea that metallic nanoparticles do not induce new SPPs/SPhPs in the surfaces while dielectric nanoparticles such as BN produce new SPhP in the material.

4. Conclusion

We have demonstrated that nanoparticles influence the emission spectra of the multilayered structures. Wavelength selectivity can be altered and controlled by the size and/or volume fraction of the NPs. The presence of NPs in a host material gives rise to an appearance of new emission peaks and a shift in the existing peaks in the emission spectra. When the metallic NPs are used, the effect of size is stronger as the dielectric function of metallic NPs has a strong dependence of particle size due to electron scattering. We have also shown that the volume fraction of the nanoparticles plays an important role in the near-field radiative heat transfer. If the NPs support SPhP, wavelength selectivity of thin films in the far field is at the locations where the real part of effective refractive index of the mixture becomes zero or the imaginary part of refractive index is small while the real part of the index is large. If the material of inclusion supports SPPs, as in metallic nanoparticles multiple emission peaks are seen which cannot be related to n- and κ-values of the mixtures. (Our observation is limited to the case where the host material is thin film.)

In the near field, for NPs supporting SPhPs or SPPs the heat transfer is nearly monochromatic around the wavelength at which n for the mixture becomes zero. It is observed that only SPhP supporting inclusions can influence the location of λ_n of the mixture; hence wavelength selectivity of thin films in the near field has little or no effect due to the presence of metallic nanoparticles. This can be understood as the presence of NPs in the thin film does not induce new kind of SPPs/SPhPs resonance across the interfaces. This work broadens the range of designs and methods for wavelength-selective emitters in both the far-field and the near-field regime.

Acknowledgements

This work is partially funded by the Rhode Island STAC Research Grant under grant number AWD05085 and NIH RI-INBRE Pilot Research Development Award supported in part by an Institutional Development Award (IDeA) Network for Biomedical Research Excellence from the National Institute of General Medical Sciences of the National Institutes of Health under grant number P20GM103430.

Author details

Yi Zheng

Address all correspondence to: zheng@uri.edu

Department of Mechanical, Industrial and Systems Engineering, University of Rhode Island, Kingston, RI, USA

References

[1] S. Basu, Y.-B. Chen, and Z. Zhang, "Microscale radiation in thermophotovoltaic devices—a review," International Journal of Energy Research 31, 689–716 (2007).

[2] C. McDonagh, C. S. Burke, and B. D. MacCraith, "Optical chemical sensors," Chemical Reviews 108, 400–422 (2008).

[3] M. Pralle, N. Moelders, M. McNeal, I. Puscasu, A. Greenwald, J. Daly, E. Johnson, T. George, D. Choi, I. El- Kady, and R. Biswas, "Photonic crystal enhanced narrow-band infrared emitters," Applied Physics Letters 81, 4685–4687 (2002).

[4] B. Guha, C. Otey, C. B. Poitras, S. Fan, and M. Lipson, "Near-field radiative cooling of nanostructures," Nano Letters 12, 4546–4550 (2012).

[5] A. Narayanaswamy and G. Chen, "Thermal emission control with one-dimensional metallodielectric photonic crystals," Physical Review B 70, 125101 (2004).

[6] A. Narayanaswamy, J. Mayo, and C. Canetta, "Infrared selective emitters with thin films of polar materials," Applied Physics Letters 104, 183107 (2014).

[7] Y. Zheng and A. Narayanaswamy, "Patch contribution to near-field radiative energy transfer and van der Waals pressure between two half-spaces," Physical Review A 89, 022512 (2014).

[8] H. Sai, H. Yugami, Y. Akiyama, Y. Kanamori, and K. Hane, "Spectral control of thermal emission by periodic microstructured surfaces in the near-infrared region," JOSA A 18, 1471–1476 (2001).

[9] P. Bermel, M. Ghebrebrhan, M. Harradon, Y. X. Yeng, I. Celanovic, J. D. Joannopoulos, and M. Soljacic, "Tailoring photonic metamaterial resonances for thermal radiation," Nanoscale Research Letters 6, 1–5 (2011).

[10] J.-P. Mulet, K. Joulain, R. Carminati, and J.-J. Greffet, "Enhanced radiative heat transfer at nanometric distances," Microscale Thermophysical Engineering 6, 209–222 (2002).

[11] Y. Zheng and A. Ghanekar, "Radiative energy and momentum transfer for various spherical shapes: a single sphere, a bubble, a spherical shell and a coated sphere," Journal of Applied Physics 117, 064314 (2015).

[12] M. Francoeur, S. Basu, and S. J. Petersen, "Electric and magnetic surface polariton mediated near-field radiative heat transfer between metamaterials made of silicon carbide particles," Optics Express 19, 18774–18788 (2011).

[13] S. J. Petersen, S. Basu, B. Raeymaekers, and M. Francoeur, "Tuning near-field thermal radiative properties by quantifying sensitivity of Mie resonance-based metamaterial design parameters," Journal of Quantitative Spectroscopy and Radiative Transfer 129, 277–286 (2013).

[14] H. Gonome, M. Baneshi, J. Okajima, A. Komiya, N. Yamada, and S. Maruyama, "Control of thermal barrier performance by optimized nanoparticle size and experimental evaluation using a solar simulator," Journal of Quantitative Spectroscopy and Radiative Transfer 149, 81–89 (2014).

[15] H. Gonome, M. Baneshi, J. Okajima, A. Komiya, and S. Maruyama, "Controlling the radiative properties of cool black-color coatings pigmented with CuO submicron particles," Journal of Quantitative Spectroscopy and Radiative Transfer 132, 90–98 (2014).

[16] J. M. Garnett, "Colours in metal glasses, in metallic films, and in metallic solutions. II," Philosophical Transactions of the Royal Society of London. Series A, Containing Papers of a Mathematical or Physical Character, pp. 237–288 (1906).

[17] W. T. Doyle, "Optical properties of a suspension of metal spheres," Physical Review B 39, 9852 (1989).

[18] C.-H. Wang, W.-Y. Shen, P.-S. Sheng, C.-Y. Lee, and H.-T. Chiu, "Deposition of mesoporous silicon carbide thin films from (me3si) 4sn: tin nanoparticles as in situ generated templates," Chemistry of Materials 19, 5250–5255 (2007).

[19] H. Wei and H. Eilers, "Electrical conductivity of thin-film composites containing silver nanoparticles embedded in a dielectric fluoropolymer matrix," Thin Solid Films 517, 575–581 (2008).

[20] W. C. Chew, "Waves and fields in inhomogeneous media," vol. 522. New York, USA: IEEE Press (1995).

[21] M. Moharam, D. A. Pommet, E. B. Grann, and T. Gaylord, "Stable implementation of the rigorous coupled-wave analysis for surface-relief gratings: enhanced transmittance matrix approach," JOSA A 12, 1077–1086 (1995).

[22] M. Planck, The theory of heat radiation (Dover Publications, 2011).

[23] A. Narayanaswamy and Y. Zheng, "A Green's function formalism of energy and momentum transfer in fluctuational electrodynamics," Journal of Quantitative Spectroscopy and Radiative Transfer 132, 12–21 (2014).

[24] V. Myroshnychenko, J. Rodr'ıguez-Ferna'ndez, I. Pastoriza-Santos, A. M. Funston, C. Novo, P. Mulvaney, L. M. Liz-Marza'n, and F. J. G. de Abajo, "Modelling the optical response of gold nanoparticles," Chemical Society Reviews 37, 1792–1805 (2008).

[25] U. Kreibig and M. Vollmer, Optical properties of metal clusters, vol. 25 (Springer, Berlin, 1995).

[26] M. S. Wheeler, "A scattering-based approach to the design, analysis, and experimental verification of magnetic metamaterials made from dielectrics," PhD thesis (2010).

[27] X. Liu, T. Bright, and Z. Zhang, "Application conditions of effective medium theory in near-field radiative heat transfer between multilayered metamaterials," Journal of Heat Transfer 136, 092703 (2014).

[28] B. Liu and S. Shen, "Broadband near-field radiative thermal emitter/absorber based on hyperbolic metamaterials: Direct numerical simulation by the wiener chaos expansion method," Physical Review B 87, 115403 (2013).

[29] E. D. Palik, Handbook of optical constants of solids, vol. 3. London, UK: Academic Press (1998).

[30] B. Neuner III, D. Korobkin, C. Fietz, D. Carole, G. Ferro, and G. Shvets, "Midinfrared index sensing of pL-scale analytes based on surface phonon polaritons in silicon carbide," The Journal of Physical Chemistry C 114, 7489–7491 (2010).

[31] P. B. Johnson and R.-W. Christy, "Optical constants of the noble metals," Physical Review B 6, 4370 (1972).

[32] V. C. Nguyen, L. Chen, and K. Halterman, "Total transmission and total reflection by zero index metamaterials with defects," Physical Review Letters 105, 233908 (2010).

[33] Y. He and T. Zeng, "First-principles study and model of dielectric functions of silver nanoparticles," The Journal of Physical Chemistry C 114, 18023–18030 (2010).

[34] K. L. Kelly, E. Coronado, L. L. Zhao, and G. C. Schatz, "The optical properties of metal nanoparticles: the influence of size, shape, and dielectric environment," The Journal of Physical Chemistry B 107, 668–677 (2003).

[35] H. Hö vel, S. Fritz, A. Hilger, U. Kreibig, and M. Vollmer, "Width of cluster plasmon resonances: bulk dielectric functions and chemical interface damping," Physical Review B 48, 18178 (1993).

[36] V. A. Parsegian, Van der Waals forces: a handbook for biologists, chemists, engineers, and physicists Cambridge, UK: Cambridge University Press (2006).

IntechOpen